Appl. Math. J. Chinese Univ.
2024, 39(3): 416-437

Suppression and synchronization of chaos in uncertain time-delay physical system

Israr Ahmad[1,*] Muhammad Shafiq[2]

Abstract. The mechanical horizontal platform (MHP) system exhibits a rich chaotic behavior. The chaotic MHP system has applications in the earthquake and offshore industries. This article proposes a robust adaptive continuous control (RACC) algorithm. It investigates the control and synchronization of chaos in the uncertain MHP system with time-delay in the presence of unknown state-dependent and time-dependent disturbances. The closed-loop system contains most of the nonlinear terms that enhance the complexity of the dynamical system; it improves the efficiency of the closed-loop. The proposed RACC approach (a) accomplishes faster convergence of the perturbed state variables (synchronization errors) to the desired steady-state, (b) eradicates the effect of unknown state-dependent and time-dependent disturbances, and (c) suppresses undesirable chattering in the feedback control inputs. This paper describes a detailed closed-loop stability analysis based on the Lyapunov-Krasovskii functional theory and Lyapunov stability technique. It provides parameter adaptation laws that confirm the convergence of the uncertain parameters to some constant values. The computer simulation results endorse the theoretical findings and provide a comparative performance.

§1 Introduction

Chaotic systems have many exciting features, such as the strange attractor, highly complex dynamics, sensitivity to initial conditions, inner randomness, and self-similarity [1]. Chaotic signals are generally noise-like waveforms and have a broadband Fourier power spectrum. The chaotic phenomenon can be found in chemical systems [2], electric circuits [3], hybrid electric vehicles [4], gasoline engines [5], biological systems[6], and so forth. Due to the unpredictable and complex behaviors of chaotic systems, control and synchronization of chaos have shown a wide range of successful applications in many physical and engineering systems, such as electronic circuits [7], biological systems [8], aerospace technology [9], secure communications [10],

Received: 2019-06-04. Revised: 2021-10-18.
MR Subject Classification: 34C28, 34C15.
Keywords: chaotic horizontal platform system, chaos suppression, chaos synchronization, robust adaptive control, Lyapunov stability theory.
Digital Object Identifier(DOI): https://doi.org/10.1007/s11766-024-3821-5.
*Corresponding author.

and chemical system [11], among others. Various feedback control strategies have been proposed to realize the suppression and synchronization of chaos, such as the twisting controller [3], adaptive control scheme [7-8], adaptive sliding mode control (ASMC) technique [7, 9], impulsive controller design [12], active and nonlinear control strategies [13], and so forth. The MHP is an interesting system that displays a rich dynamical behavior, including regular and chaotic [14]. The MHP system can rotate freely around the horizontal axis, which penetrates its mass center. It is widely used in earthquake and offshore engineering [15]. Since the chaotic behavior of the MHP system is aperiodic and sub-harmonic which produces broadband vibrations within the system, the control and synchronization of chaos in the MHP system are essential and challenging. The relevant literature reports some interesting works that design different feedback control strategies to stabilize and synchronize chaos in the MHP system [14-18]. Using the SMC technique, the article [14] studies the suppression of chaos in the MHP system with external harmonic force and parametric uncertainties. A novel adaptive control strategy [15] is developed to study the finite-time synchronization of two identical MHP systems. The authors [16] investigate the circuit implementation and synchronization control of chaos in the MHP system. The paper [17] studies the chaotic behavior and stabilization of chaos in a fractional-order MHP system. The article [18] analyzes a new fuzzy adaptive prescribed performance controller with unknown controller gain to investigate the suppression of chaos in the MHP system.

Great efforts and expertise of the researchers have developed state-of-the-art control methodologies for the suppression and synchronization of chaos in the MHP system [14-18]. However, there are still demands for complex feedback control schemes. The design of such chaos control and synchronization techniques requires resolving the following challenging issues.

(i) The feedback controllers in [14-18] eliminate most of the nonlinear terms. Such cancellation procedures require exact knowledge of the systems' states and parameters. In practice, the measurement of the states is erroneous as well as the parameters are unknown, and their estimates are uncertain. As a result, the cancellation process leaves residual nonlinear terms in the closed-loop. Such a feedback linearized closed-loop system performs weak operations that include long time delay and sudden supply load disturbances. These factors leave adverse effects on the performance of the controlled system, and the system may lose stability [19].

(ii) In practice, some unavoidable factors exist, such as the time delay, unknown state-dependent, and time-dependent disturbances that influence the performance of the system dynamics. The effect of time delay on chaotic systems is quite remarkable [20]. Chaotic systems with time delay exhibit multi-stability and produce complex dynamics. The existence of time delay in the physical systems has received considerable attention in the relevant literature [20-22]. The increased efficiency requirements in the controller feedback control inputs have demanded analyzing time-delays' effect on the system dynamics [21]. The presence of time delay in chaotic systems, controllers, and actuators can generate erroneous feedback control behaviors that result in the instability of the closed-loop and degrade the control and synchronization performance [21-22]. It is investigated that time delay in the MHP system exhibits more complex dynamics and shows multiple chaotic regions [21]. In [14-18], the effect of time-delay is not considered for the suppression and synchronization of chaos in the MHP system.

(iii) The feedback control algorithms [14-18] produce large undesirable oscillations in the control signals that further degrade MHP systems' performance. A small delay can drive the desired orbit away from the targeted equilibrium point.

(iv) The stabilization and synchronization control approaches [14-18] provide slow converging rates of the state (error) trajectories to zero, affecting the performance of control methodology in practice.

(v) The reported controller schemes [15, 18] require the exact knowledge of the upper bounds of the unknown state-dependent and time-dependent disturbances, which is hard to determine in practice.

The suppression and synchronization of chaos in the uncertain time-delay MHP chaotic system have rarely been studied and remain an open problem. Using the Lyapunov-Krasovskii functional theory [23], this paper investigates the design of an RACC algorithm for the suppression and synchronization of chaos in the time-delay MHP system with uncertain parameters. It is assumed that the unknown state-dependent and unknown time-dependent disturbances perturb the time-delay MHP chaotic system. The proposed RACC algorithm establishes the suppression and synchronization of chaos in the uncertain time-delay MHP chaotic system. The Lyapunov direct method [24] proves the robust asymptotic stability of the closed-loop system at the origin. Trajectories of the state variables and synchronization errors converge to the origin without exhibiting overshoot. The RACC approach reduces the transient time and provides faster convergence rates. This convergence behavior is verified graphically as well as analytically. The article gives a detailed analysis of the proposed RACC technique and parameter adaptation laws. It also compares the performance of the proposed RACC algorithm with the feedback controller schemes reported in the articles [7-9]. This article has the following main contributions.

(i) Design a robust RACC algorithm that investigates the control and synchronization of chaos in the uncertain MHP system with time delay. This controller establishes the robust asymptotic stability of the closed-loop system at the origin.

(ii) The proposed RACC strategy reduces the transient time, increases the convergence rates, and suppresses chattering in the control input signals.

(iii) The computer-based simulation results certify the efficiency and performance of the proposed RACC approach and compare them with peer works [7-9].

The remaining article is organized as follows: In section 2, this paper presents the chaotic MHP system dynamics and states some preliminaries. Section 3 demonstrates the problems for the suppression and synchronization of chaos in the uncertain MHP chaotic system with time delay and parametric uncertainties. Sections 4 and 5 provide solutions to Section 3 and simulation results with a comparative study. The paper ends with the conclusions in Section 6.

§2 Chaotic Dynamics of the Mechanical Horizontal Platform System

2.1 Symbols and notations

The paper uses symbols and notations described in Table 1.

Table 1. Symbols and notations.

Symbols	Description
$\mathbf{A}$ and $\mathbf{a}$	$\mathbf{A}$ denotes an $n \times n$ matrix whereas $\mathbf{a}$ represents an $n \times 1$ vector
R	Real numbers
T	Transpose of a matrix(vector)
$\mathbf{x}(t) = [x_1(t) \quad x_2(t)]^T \in R^{2\times 1}$	State variables vector of the MHP chaotic system (2)
α, β, γ, and δ	Constant parameters of the MHP chaotic system (2)
$\tau \in R^+$	Constant time-delay
$\vartheta(\mathbf{x}(t))$=$\{\vartheta_{ij}(x_i(t)),\, i,j = 1,2 \Rightarrow \vartheta_{ij}(x_i(t)) = 0\}$ $\in R^{2\times 2}$	Unknown time-varying model uncertainties present in the MHP chaotic system (2)
$\varphi(t)$=$\{\varphi_{ij}(t),\, i,j = 1,2 \Rightarrow \varphi_{ij}(t) = 0\} \in R^{2\times 2}$	Unknown external disturbances acting on the MHP chaotic system (2)
ϑ_m=$\{\vartheta_{mij} \in R^+,\, i,j = 1,2 \Rightarrow \vartheta_{mij} = 0\} \in R^{2\times 2}$, and φ_m=$\{\varphi_{mij} \in R^+,\, i,j = 1,2 \Rightarrow \varphi_{mij} = 0\} \in R^{2\times 2}$	ϑ_m and φ_m are the matrices of the least upper bound of $\vartheta(\mathbf{x}(t))$ and $\varphi(t)$, respectively
$\mathbf{u}(t) = [u_1(t) \quad u_2(t)]^T \in R^{2\times 1}$	Control input vector
$\mathbf{K}$=$\{k_{ij},\, i,j = 1,2 \Rightarrow k_{ij} = 0\} \in R^{2\times 2}$, and $\mathbf{L}$=$\{l_{ij},\, i,j = 1,2 \Rightarrow l_{ij} = 0\} \in R^{2\times 2}$	Feedback controller gain matrices
$\hat{\vartheta}(t)$=$\{\hat{\vartheta}_{ij}(t) \in R^+,\, i,j = 1,2 \Rightarrow \hat{\vartheta}_{ij}(t) = 0\}$ $\in R^{2\times 2}$, and $\hat{\varphi}(t)$=$\{\hat{\varphi}_{ij}(t) \in R^+,\, i,j = 1,2 \Rightarrow \hat{\varphi}_{ij}(t) = 0\}$ $\in R^{2\times 2}$	Unknown bounded controller parameters in (23)
$\rho,\, \sigma,\, \eta \in R^+$, $\rho > 0$, and $0 < \eta, \sigma \leq 1$	Controller parameters
$\varrho,\, \lambda \in R^+$	Positive real constants
e	The base of the natural logarithm
$sgn(.)$	Signum function

2.2 Mechanical horizontal platform chaotic system

The MHP chaotic system is a subject of great interest due to its rich complex dynamical behavior and has been extensively studied in the relevant literature. The chaotic MHP system can be utilized in various engineering applications, including earthquake and offshore industries [14]. The MHP system consists of an accelerometer and a platform located, as shown in Fig. 1. An accelerometer is placed on the left side of the platform. When the platform moves away from the horizon, the accelerometer produces an output signal to the actuator. It generates a torque to reverse the platforms' rotation that balances the MHP system to its original position [14-18]. The mathematical equation governing the chaotic dynamics of the MHP system [15] can be described as follows:

$$A\ddot{x}(t) + B\dot{x}(t) + rg\, sin(t) - 3\frac{g}{R}(C - D)cos(t)\, sin(t) \quad = \quad F cos\, \omega t, \tag{1}$$

where $x(t)$ represents the rotation of the platform relative to the earth, $A = 0.3, B = 0.5$, and $D = 0.2$ represent the moment of inertia for axes $1, 2$, and 3, alternatively. $g = 9.8$ is the gravitational acceleration, $C = 0.4$ denotes the damping coefficient, $r = 0.1155633$ represents

the constant of accelerometer, $R = 6.378$ indicates the radius of the earth, and $F cos\,\omega t$ denotes the harmonic torque with $F = 3.4$, and $\omega = 1.8$.
Define $[x\,(t) \quad \dot{x}\,(t)]^T$=$[x_1\,(t) \quad x_2\,(t)]^T$, then the equations of motion of the non-autonomous MHP chaotic system is given by:

$$\mathbf{x}\,(t) = \begin{cases} \dot{x}_1\,(t) = x_2\,(t) \\ \dot{x}_2\,(t) = -\alpha\, x_2\,(t) - \beta\, cosx_1\,(t) + \gamma\, sinx_1\,(t)\, cosx_1\,(t) + \delta\, cos\omega t \end{cases} \tag{2}$$

Fig. 1 shows the physical model of the MHP system.

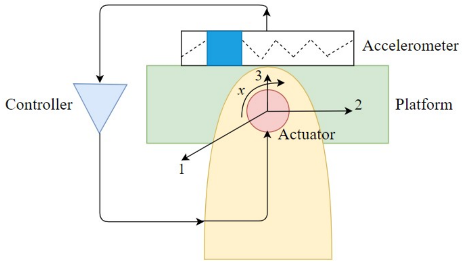

Figure 1. Physical model of the MHP system.

2.3 Preliminaries

The following statements, assumptions, and lemmas are essential for this work.
(i) For $A, B \in R$, the following inequality holds:

$$|cosAsinB| = |cosA||sinB| \leq 1. \tag{3}$$

(ii) It follows from the differential mean-value theorem [25] that:

$$\frac{\sin B - \sin A}{(B - A)} = \cos\theta,$$

where, $\theta \in [A, B]$ and $(A < B)$.
This implies that:

$$sinB - sinA = (B - A)\cos\theta \tag{4}$$

(iii) For $A \in R$, the following trigonometric identity holds:

$$2sinAcosA = sin2A \tag{5}$$

Lemma 2.1. For any non-negative real numbers P and Q:

$$\frac{P^2}{2} + \frac{Q^2}{2} \geq PQ. \tag{6}$$

Proof. Let P and Q are any non-negative real numbers, then the following identity holds:
$(P - Q)^2 \geq 0 = P^2 + Q^2 - 2PQ \geq 0 \Rightarrow P^2 + Q^2 \geq 2PQ$
$\Rightarrow$

$$\frac{P^2}{2} + \frac{Q^2}{2} \geq PQ. \tag{7}$$

Lemma 2.2. For a positive real constant A and given a scalar B, the following identity holds:

$$A\tanh AB = |A\tanh AB| = |A||\tanh AB| \geq 0. \tag{8}$$

Proof. From the definition of tanh(.), we have:

$$A \tanh AB = A \frac{2}{e^{AB} + e^{-AB}}. \tag{9}$$

Multiply right-hand side of (9) by $\frac{e^{AB}}{e^{-AB}}$ yields:

$$A \tanh AB = A \left(\frac{1}{1 + e^{2AB}} \right) \left(e^{2AB} - 1 \right). \tag{10}$$

Now, if;

$$\begin{cases} \left(e^{2AB} - 1 \right) \geq 0, & if \;\; B \geq 0, \\ \left(e^{2AB} - 1 \right) < 0, & if \;\; B < 0, \end{cases} \tag{11}$$

then, the following inequality can be obtained:

$$\left(e^{2AB} - 1 \right) \leq 0. \tag{12}$$

Since, $\left(\frac{1}{1+e^{2AB}} \right) > 0$ and using (12) gives:

$$A \tanh AB = A \left(\frac{1}{1 + e^{2AB}} \right) \left(e^{2AB} - 1 \right) \geq 0. \tag{13}$$

Thus, for all positive A and a scalar B, if $AB \geq 0$, then $AB = |AB| = |A||B| \geq 0$ is true. Consequently, it concludes that:

$$A \tanh AB = |A \tanh AB| = |A| |\tanh AB| \geq 0. \tag{14}$$

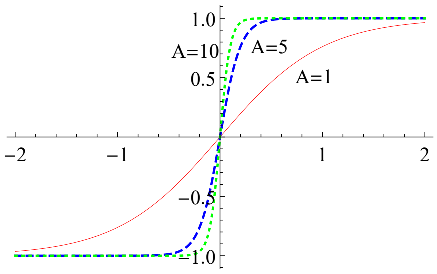

Figure 2. Behavior of the $tanh(.)$ with different values of A.

Remark 3.1. In (14), the positive real constant A represents the steepness of the tanh(.), as shown in Fig. 2.

§3 Problems Formulation: Suppression and Synchronization of Chaos in the Uncertain Horizontal Platform System with Time-Delay

3.1 Problem 1: Suppression of chaos in the uncertain MHP chaotic system with time-delay

Most digital controllers, reconstruction filters, and analog antialiasing exhibit an inevitable time delay during the process. Similarly, the human-machine and hydraulic actuators interaction show significant time-delay [21]. Therefore, it is interesting to study the suppression and synchronization of the MHP system with constant time-delay. This subsection presents the problem formulation to suppress chaos in the MHP chaotic system with time-delay τ and uncertain parameters. Let us introduce a constant time delay in the feedback of the state variable $x_2(t)$ and consider the following controlled MHP chaotic system when unknown state-dependent disturbances $\vartheta_{ii}(x_i(t))$, unknown times-dependent disturbances $\varphi_{ii}(t)$, and a control effort $\mathbf{u}(t) \in R^{2\times 1}$ act on the MHP chaotic system (2). Then (15) represents the closed-loop dynamics.

$$\mathbf{x}(t) = \begin{cases} \dot{x}_1(t) = x_2(t) + \vartheta_{11}(x_1(t)) + \varphi_{11}(t) + u_1(t) \\ \dot{x}_2(t) = -\alpha\, x_2(t-\tau) - \beta\, cosx_1(t) + \gamma\, sinx_1(t)\, cosx_1(t) \\ \qquad + \delta\, cos\omega t + \vartheta_{22}(x_2(t)) + \varphi_{22}(t) + u_2(t) \,. \end{cases} \tag{15}$$

Assumptio 3.1. The evolvement of a chaotic attractor in the bounded region assures the boundedness of the chaotic trajectories; it implies the boundedness of $\vartheta_{ii}(x_{ii}(t))$. In general, it is also presumed that the unknown time-dependent disturbance signal $\varphi_{ii}(t)$ is the norm-bounded in C^1 [8]. Therefore, there exist unknown positive real constants ϑ_{mii} and φ_{mii} such that:

$$|\vartheta_{ii}(x_{ii}(t))| \leq \vartheta_{mii} \quad and \quad |\varphi_{ii}(t)| \leq \varphi_{mii}, i = 1, 2, \tag{16}$$

where ϑ_{mii} and φ_{mii} are upper bounds of the unknown state-dependent and time-dependent disturbances in (16), respectively, which are unknown.

In this situation, it is desired to synthesize feedback control input vector $\mathbf{u}(t)$ that assures the smooth and fast convergence of the closed-loop system (15) trajectories to the origin and realizes the robust asymptotic stability of the equilibrium point at the origin with a sense that $\lim\limits_{t\to\infty} \|\mathbf{x}(t)\| = 0$.

3.2 Problem 2: Synchronization of two identical uncertain MHP chaotic systems with time-delay

This subsection presents the problem formulation to synchronize two identical uncertain MHP chaotic systems with constant time delay. Consider two coupled uncertain time-delay MHP chaotic systems, where $\mathbf{x}(t)$ and $\mathbf{y}(t)$ are vectors that represent states of the master and slave uncertain time-delay MHP chaotic systems, respectively. Equations (17-18) describe the master-slave system (MSS) arrangement when unknown state-dependent disturbances $\vartheta_{ii}^{M}(x_{ii}(t))$ and $\vartheta_{ii}^{S}(y_{ii}(t))$ and unknown time-dependent disturbances $\varphi_{ii}^{M}(t)$ and $\varphi_{ii}^{S}(t)$ act on the MSS (17-18), respectively.

(Master time-delay MPH chaotic system)

$$\mathbf{x}(t) = \begin{cases} \dot{x}_1(t) = x_2(t) + \vartheta_{11}^{M}(x_1(t)) + \varphi_{11}^{M}(t) \\ \dot{x}_2(t) = -\alpha\, x_2(t-\tau) - \beta\, cosx_1(t) + \gamma\, sinx_1(t)\, cosx_1(t) \\ \qquad + \delta\, cos\omega t + \vartheta_{11}\left(x_1^{M}(t)\right) + \varphi_{11}^{M}(t) \end{cases} \tag{17}$$

(Slave time-delay MPH chaotic system)

$$\mathbf{y}(t) = \begin{cases} \dot{y}_1(t) = x_2(t) + \vartheta_{11}^{S}(x_1(t)) + \varphi_{11}^{S}(t) + u_1(t) \\ \dot{y}_2(t) = -\alpha\, x_2(t-\tau) - \beta\, cosx_1(t) + \gamma\, siny_1(t)\, cosy_1(t) \\ \qquad + \delta\, cos\omega t + \vartheta_{22}^{S}(x_2(t)) + {\varphi_{22}}^{S}(t) + u_2(t) \end{cases} \tag{18}$$

Taking $e_i(t) = y_i(t) - x_i(t)$. Then, (19) gives the dynamical error system for the MSS (17-18).

$$\mathbf{e}(t) = \begin{cases} \dot{e}_1(t) = e_2(t) + H_{11}(t) + u_1(t) \\ \dot{e}_2(t) = -\alpha\, e_2(t-\tau) - \beta\,(siny_1(t) - sinx_1(t)) + H_{22}(t) \\ \qquad + \gamma\,(siny_1(t)\,cosy_1(t) - sinx_1(t)\,cosx_1(t)) + u_2(t), \end{cases} \tag{19}$$

where $H_{ii}(t) = \vartheta_{ii}^{M}(y_i(t)) - \vartheta_{ii}^{S}(x_i(t)) + {\varphi_{ii}}^{S}(t) - {\varphi_{ii}}^{M}(t), i = 1, 2.$
Using (4) and (5), the error dynamical system (19) becomes:

$$\mathbf{e}(t) = \begin{cases} \dot{e}_1(t) = e_2(t) + H_{11}(t) + u_1(t) \\ \dot{e}_2(t) = -\alpha\, e_2(t-\tau) - \beta\, e_1(t)\, cos\theta \\ \qquad + \dfrac{\gamma}{2}(sin2y_1(t) - sin2x_1(t)) + H_{22}(t) + u_2(t) \end{cases} \tag{20}$$

Assumptio 3.2. Following Assumption 1, there exist positive real constants ϑ_{ii}^{M}, ϑ_{ii}^{S}, ${\varphi_{ii}}^{M}$, and ${\varphi_{ii}}^{S}$ such that:

$$\begin{gathered} |\vartheta_{ii}^{M}(x_i(t))| \leq \vartheta_{mii}^{S}, \ \ |\vartheta_{ii}^{S}(x_i(t))| \leq \vartheta_{mii}^{M}, \\ |\varphi_{ii}^{M}(t)| \leq \varphi_{mii}^{M}, \ \ and \ \ |\varphi_{ii}^{S}(t)| \leq \varphi_{mii}^{S}, i = 1, 2, \end{gathered} \tag{21}$$

Hence, it is concluded that

$$|\vartheta_{ii}\left(y_i^{S}(t)\right) - \vartheta_{ii}\left(x_i^{M}(t)\right)| \leq \vartheta_{mii}, \ \ and \ \ |\varphi_{ii}(t) - \varphi_{ii}^{S}(t)| \leq \varphi_{mii}, i = 1, 2, \tag{22}$$

where ϑ_{mii} and φ_{mii} are upper bounds of the unknown state-dependent and time-dependent disturbances in (20) and (21), respectively. Therefore, without loss of generality, it is assumed that $\vartheta_{mii} = \varphi_{mii}, i = 1, 2.$

§4 Solution to Problem 1

4.1 Controller design

To stabilize the uncertain time-delay MHP chaotic system (15) at the origin, let us define the following RACC functions:

$$\mathbf{u}(t) = \begin{cases} u_1(t) = -k_{11}x_1(t) - L_{11}(t)\tanh\rho x_1(t) + \left(\hat{\vartheta}_{m11}(t) + \hat{\varphi}_{m11}(t)\right)\tanh\rho x_1(t) \\ u_2(t) = -k_{22}x_2(t) - L_{22}(t)\tanh\rho x_2(t) + \left(\hat{\vartheta}_{m22}(t) + \hat{\varphi}_{m22}(t)\right)\tanh\rho x_2(t), \\ \qquad + \hat{\alpha}(t)\,x_2(t-\tau) + \hat{\beta}(t)\,cosx_1 + \hat{\gamma}(t)\,sinx_1cosx_1 - \delta\, cos\,\omega t, \end{cases} \tag{23}$$

where $L(t) = [L_{ij}(t), L_{ij}(t) = 0 \ \ for \ \ i \neq j]_{2\times 2}$ and $L_{ii}(t) = [l_{ii}\left(I_{ii} - \eta e^{-\sigma|x_i(t)|}\right)]_{2\times 2}$, $\hat{\alpha}(t), \hat{\beta}(t), \hat{\gamma}(t), \ \hat{\vartheta}_{mii}(t)$, and $\hat{\varphi}_{mii}(t), i = 1, 2$ are the adaptation parameters. k_{ii} and $L_{ii}(t)$, $i = 1, 2$ are the feedback gains.

There are three fundamental components of the feedback controller in (23). The following items summarize the role of these components.

(i) The linear term $k_{ii}x_i(t)$ stabilizes the closed-loop.

(ii) The nonlinear term $L_{ii}(t)\tanh\rho x_i(t)$ provides smooth and fast convergence of the state vector trajectories to the origin. $L_{ii}(t)$ is a variable gain given by $L_{ii} - \rho L_{ii} \leq L_{ii}(t) \leq L_{ii}$.

(iii) The nonlinear adaptive term $\left(\hat{\vartheta}_{mii}(t) + \hat{\varphi}_{mii}(t)\right)\tanh\rho x_i(t)$ eradicates the effects of time-varying unknown model uncertainties, external disturbances and suppresses chattering in the control input signals.

Remark 4.1. The proposed controller (23) introduces the smooth continuous tanh function that suppresses chattering in the control inputs. The controller eradicates the adverse effect induced by the time-delay, uncertain parameters, unknown state-dependent disturbances, and unknown time-dependent disturbances. It stabilizes the closed-loop (23) at the origin with faster-converging rates. The parameters k_{ii}, l_{ii}, σ, and η provide complete control over the transient time and convergence rates. Larger values of k_{ii}, l_{ii}, σ, and η provide faster convergence rates.

4.2 Robust asymptotic stability analysis

This sub-section analyses the main claim that the perturbed state variables converge to the equilibrium point of the closed-loop.

Theorem 4.1. If the feedback control signals (23) are applied to (15), and the parameter adaptation laws are given by (24), then the closed-loop system (15) is asymptotically stable at the origin.

$$\begin{cases} \dot{\hat{\alpha}}(t) = -\varrho x_2(t-\tau)\, x_2(t), \dot{\hat{\beta}}(t) = -\varrho x_2(t), \dot{\hat{\gamma}}(t) = \varrho x_2(t)\, cosx_1(t)\, sinx_1(t), \\ \dot{\hat{\vartheta}}_{ii}(t) = \dot{\hat{\varphi}}_{ii}(t) = -\varrho |x_i(t)|, \hat{\alpha}(0) = \hat{\alpha}_0, \hat{\beta}(0) = \hat{\beta}_0, \hat{\gamma}(0) = \hat{\gamma}_0, \hat{\vartheta}_{ii}(0) = \hat{\vartheta}_{ii0}, \\ \hat{\varphi}_{ii}(0) = \hat{\varphi}_{ii0}, i = 1, 2, \end{cases} \tag{24}$$

where $\hat{\alpha}_0$, $\hat{\beta}_0$, $\hat{\gamma}_0$, $\hat{\vartheta}_{ii0}$ and $\hat{\varphi}_{ii0}$ are the initial values of $\hat{\alpha}(t)$, $\hat{\beta}(t)$, $\hat{\gamma}(t)$, $\hat{\vartheta}_{ii}(t)$, and $\hat{\varphi}_{ii}(t)$, alternatively.

Proof. Consider the following Lyapunov functional as:

$$V(\mathbf{x}(t)) = \begin{array}{l} \frac{\varrho}{2}\mathbf{x}^T(t)\,\mathbf{x}(t) + \frac{1}{2}\left(\hat{\alpha}^2(t) + \hat{\beta}^2(t) + \hat{\gamma}^2(t)\right) \quad + \frac{1}{2}\sum_{n=1}^{\infty}\left(\tilde{\vartheta}_{mii}(t)\,\vartheta_{mii} + \tilde{\varphi}_{mii}(t)\,\varphi_{mii}\right) \\ + \frac{\lambda}{2}\int_{t-\tau}^{t} x_2^2(t)\, dt \geq 0, \end{array} \tag{25}$$

provided $|\tilde{\vartheta}_{mii}(t)| \leq \vartheta_{mii}$ and $|\tilde{\varphi}_{mii}(t)| \leq \varphi_{mii}$, where $\tilde{\vartheta}_{mii}(t) = \vartheta_{mii} + \hat{\vartheta}_{mii}(t)$, $\tilde{\varphi}_{mii}(t) = \varphi_{mii} + \hat{\varphi}_{mii}(t)$, and $\tilde{\alpha}(t) = \hat{\alpha}(t) - \alpha$, $\tilde{\beta}(t) = \hat{\beta}(t) - \beta$, and $\tilde{\gamma}(t) = \hat{\gamma}(t) - \gamma$.

Remark 4.2. $\tilde{\vartheta}_{ii}(t)\,\vartheta_{mii} \geq 0$ and $\tilde{\varphi}_{mii}(t)\,\varphi_{mii} \geq 0$ when $|\hat{\vartheta}_{mii}(t)| \leq \vartheta_{mii}$ and $|\hat{\varphi}_{mii}(t)| \leq \varphi_{mii}$, it requires that $\lim_{t\to\infty}\hat{\vartheta}_{mii}(t) = -\vartheta_{mii}$ and $\lim_{t\to\infty}\hat{\varphi}_{mii}(t) = -\varphi_{mii}$ without oscillations. Therefore, (25) holds. Parameter adaptation laws (24) assure that $\hat{\vartheta}_{mii}(t) \leq 0$ and $\hat{\varphi}_{mii}(t) \leq 0$ for $\hat{\vartheta}_{mii}(0) = \hat{\vartheta}_{mii}(0) = 0$.

The derivative of (25) along (15) gives:

$$\begin{aligned} \dot{V}(\mathbf{x}(t)) &= \varrho x_1(t)\,(x_2(t) + \vartheta_{11}(x_1(t)) + \varphi_{11}(t) + u_1(t)) \\ &+ \varrho x_2(t)\,(-\alpha\, x_2(t-\tau) - \beta\, cosx_1(t) + \gamma\, sinx_1(t)\, cosx_1(t) \\ &+ \delta\, cos\omega t + \vartheta_{22}(x_2(t)) + \varphi_{22}(t) + u_2(t)) \\ &+ \tilde{\alpha}(t)\,\dot{\hat{\alpha}}(t) + \tilde{\beta}(t)\,\dot{\hat{\beta}}(t) + \tilde{\gamma}(t)\,\dot{\hat{\gamma}}(t) + \lambda x_2^2(t) - \lambda x_2^2(t-\tau) \\ &+ \sum_{n=1}^{\infty}\left(\vartheta_{mii}\dot{\hat{\vartheta}}_{mii}(t) + \varphi_{mii}\dot{\hat{\varphi}}_{mii}(t)\right) \end{aligned}$$

$$
\begin{aligned}
&= \varrho x_1(t)\,x_2(t) - \alpha\varrho x_2(t-\tau)\,x_2(t) - \varrho\beta x_2(t)\,cosx_1(t) + \varrho\delta\,x_2(t)\,cos\omega t\\
&+ \varrho\gamma x_2(t)\,cosx_1(t)\,sinx_1(t) + \tilde{\alpha}(t)\,\dot{\hat{\alpha}}(t) + \tilde{\beta}(t)\,\dot{\hat{\beta}}(t) + \tilde{\gamma}(t)\,\dot{\hat{\gamma}}(t)\\
&+ \varrho\sum_{n=1}^{\infty}\left(\vartheta_{mii}(x_i(t)) + \varphi_{mii}(t)\right)x_i(t) + \sum_{n=1}^{\infty}\left(\vartheta_{mii}\dot{\hat{\vartheta}}_{mii}(t) + \varphi_{mii}\dot{\hat{\varphi}}_{mii}(t)\right)\\
&+ \lambda x_2^2(t) - \lambda x_2^2(t-\tau) + \varrho\sum_{n=1}^{\infty}x_i(t)\,u_i(t)\\
&\le \varrho|x_1(t)\,x_2(t)| - \varrho x_2(t-\tau)\,x_2(t) - \varrho\beta x_2(t)\,cosx_1(t) + \varrho\delta\,x_2(t)\,cos\omega t\\
&+ \varrho\gamma x_2(t)\,cosx_1(t)\,sinx_1(t) + \tilde{\alpha}(t)\,\dot{\hat{\alpha}}(t) + \tilde{\beta}(t)\,\dot{\hat{\beta}}(t) + \tilde{\gamma}(t)\,\dot{\hat{\gamma}}(t)\\
&+ \varrho\sum_{n=1}^{\infty}\left(\vartheta_{mii}(x_i(t)) + \varphi_{mii}(t)\right)x_i(t) + \sum_{n=1}^{\infty}\left(\vartheta_{mii}\dot{\hat{\vartheta}}_{mii}(t) + \varphi_{mii}\dot{\hat{\varphi}}_{mii}(t)\right)\\
&+ \lambda x_2^2(t) - \lambda x_2^2(t-\tau) + \varrho\sum_{n=1}^{\infty}x_i(t)\,u_i(t)\,.
\end{aligned}
\tag{26}
$$

Using Assumption 1, Lemma 1, and substituting the feedback control inputs (23) into (26) implies:

$$
\begin{aligned}
&\dot{V}(\mathbf{x}(t)) \le \frac{\varrho}{2}\left(x_1^2(t) + x_2^2(t)\right) - \varrho\sum_{n=1}^{\infty}k_{ii}x_i^2(t) - \varrho\sum_{n=1}^{\infty}L_{ii}(t)\,x_i(t)\tanh\rho x_i(t)\\
&+ \lambda x_2^2(t) - \lambda x_2^2(t-\tau) + \varrho\hat{\alpha}(t)\,x_2(t-\tau)\,x_2(t) - \varrho\alpha x_2(t-\tau)\,x_2(t)\\
&+ \varrho\hat{\beta}(t)\,x_2(t)\,cosx_1(t) - \varrho\beta x_2(t)\,cosx_1(t) - \varrho\hat{\gamma}(t)\,x_2(t)\,cosx_1(t)\,sinx_1(t)\\
&+ \varrho\gamma x_2(t)\,cosx_1(t)\,sinx_1(t) + \tilde{\alpha}(t)\,\dot{\hat{\alpha}}(t) + \tilde{\beta}(t)\,\dot{\hat{\beta}}(t) + \tilde{\gamma}(t)\,\dot{\hat{\gamma}}(t)\\
&+ \varrho\sum_{n=1}^{\infty}\left(\vartheta_{mii}(x_i(t)) + \varphi_{mii}(t)\right)x_i(t) + \sum_{n=1}^{\infty}\left(\vartheta_{mii}\dot{\hat{\vartheta}}_{mii}(t) + \varphi_{mii}\dot{\hat{\varphi}}_{mii}(t)\right)\\
&+ \varrho\sum_{n=1}^{\infty}\left(\hat{\vartheta}_{mii}(t) + \hat{\varphi}_{mii}(t)\right)x_i(t)\tanh\rho x_i(t)\\
&\le -\varrho\sum_{n=1}^{\infty}k_{ii}x_i^2(t) - \varrho\sum_{n=1}^{\infty}L_{ii}(t)\,x_i(t)\tanh\rho x_i(t) + \frac{\varrho}{2}\left(x_1^2(t) + x_2^2(t)\right) + \lambda x_2^2(t)\\
&- \lambda x_2^2(t-\tau) + \varrho x_2(t-\tau)\,x_2^2(t) + \varrho\left(\hat{\alpha}(t) - \alpha\right)x_2(t-\tau)\,x_2(t)\\
&+ \varrho\left(\hat{\beta}(t) - \beta\right)x_2(t)\,sinx_1(t) - \varrho\left(\hat{\gamma}(t) - \gamma\right)x_2(t)\,cosx_1(t)\,sinx_1(t)\\
&+ \tilde{\alpha}(t)\,\dot{\hat{\alpha}}(t) + \tilde{\beta}(t)\,\dot{\hat{\beta}}(t) + \tilde{\gamma}(t)\,\dot{\hat{\gamma}}(t) + \varrho\sum_{n=1}^{\infty}\left(\vartheta_{mii}(x_i(t)) + \varphi_{mii}(t)\right)x_i(t)\\
&+ \sum_{n=1}^{\infty}\left(\vartheta_{mii}\dot{\hat{\vartheta}}_{mii}(t) + \varphi_{mii}\dot{\hat{\varphi}}_{mii}(t)\right) + \varrho\sum_{n=1}^{\infty}\left(\hat{\vartheta}_{mii}(t) + \hat{\varphi}_{mii}(t)\right)x_i(t)\tanh\rho x_i(t)\\
&\le -\varrho\left(k_{11} - \frac{1}{2}\right)x_1^2(t) - \varrho\left(k_{22} - \frac{\lambda}{2} - \frac{1}{2}\right)x_2^2(t) - \varrho\sum_{n=1}^{\infty}L_{ii}(t)\,x_i(t)\tanh\rho x_i(t)\\
&- \lambda x_2^2(t-\tau) + \tilde{\alpha}(t)\left(\dot{\hat{\alpha}}(t) + \varrho x_2(t-\tau)\,x_2(t)\right) + \tilde{\beta}(t)\left(\dot{\hat{\beta}}(t) + \rho x_2(t)\right)\\
&+ \tilde{\gamma}(t)\left(\dot{\hat{\gamma}}(t) - \rho x_2(t)\,cosx_1(t)\,sinx_1(t)\right)
\end{aligned}
$$

$$\begin{aligned}&+\sum_{n=1}^{\infty}\left(\varrho\vartheta_{mii}\left(x_i\left(t\right)\right)x_i\left(t\right)+\varrho\hat{\vartheta}_{ii}\left(t\right)x_i\left(t\right)\tanh\rho x_i\left(t\right)+\vartheta_{mii}\dot{\hat{\vartheta}}_{mii}\right)\\&+\sum_{n=1}^{\infty}\left(\varrho\varphi_{mii}\left(x_i\left(t\right)\right)x_i\left(t\right)+\varrho\hat{\varphi}_{ii}\left(t\right)x_i\left(t\right)\tanh\rho x_i\left(t\right)+\varphi_{mii}\dot{\hat{\varphi}}_{mii}\right).\end{aligned}\tag{27}$$

Substituting the value of $\dot{\hat{\alpha}}(t)$, $\dot{\hat{\beta}}(t)$, and $\dot{\hat{\gamma}}(t)$ in (27) yields:

$$\begin{aligned}\dot{V}\left(\mathbf{x}\left(t\right)\right)\le&-\varrho\left(k_{11}-\frac{1}{2}\right)x_1^2\left(t\right)-\varrho\left(k_{22}-\frac{\lambda}{2}-\frac{1}{2}\right)x_2^2\left(t\right)\\&-\varrho\sum_{n=1}^{\infty}L_{ii}\left(t\right)x_i\left(t\right)\tanh\rho x_i\left(t\right)-\lambda x_2^2\left(t-\tau\right)\\&+\sum_{n=1}^{\infty}\left(\varrho\vartheta_{mii}\left(x_i\left(t\right)\right)x_i\left(t\right)+\varrho\hat{\vartheta}_{ii}\left(t\right)x_i\left(t\right)\tanh\rho x_i\left(t\right)+\vartheta_{mii}\dot{\hat{\vartheta}}_{mii}\right)\\&+\sum_{n=1}^{\infty}\left(\varrho\varphi_{mii}\left(x_i\left(t\right)\right)x_i\left(t\right)+\varrho\hat{\varphi}_{ii}\left(t\right)x_i\left(t\right)\tanh\rho x_i\left(t\right)+\varphi_{mii}\dot{\hat{\varphi}}_{mii}\right)\end{aligned}$$

$$\dot{V}\left(\mathbf{x}\left(t\right)\right)\le\dot{V}_{KL}\left(\mathbf{x}\left(t\right)\right)+\dot{V}_{\vartheta}\left(\mathbf{x}\left(t\right)\right)+\dot{V}_{\varphi}\left(\mathbf{x}\left(t\right)\right),\tag{28}$$

where

$$\begin{aligned}\dot{V}\left(\mathbf{x}\left(t\right)\right)\le&-\varrho\left(k_{11}-\frac{1}{2}\right)x_1^2\left(t\right)-\varrho\left(k_{22}-\frac{\lambda}{2}-\frac{1}{2}\right)x_2^2\left(t\right)\\&-\varrho\sum_{n=1}^{\infty}L_{ii}\left(t\right)x_i\left(t\right)\tanh\rho x_i\left(t\right)-\lambda x_2^2\left(t-\tau\right),\end{aligned}\tag{29}$$

$$\dot{V}_{\vartheta}\left(\mathbf{x}\left(t\right)\right)=\sum_{n=1}^{\infty}\left(\varrho\vartheta_{mii}\left(x_i\left(t\right)\right)x_i\left(t\right)+\varrho\hat{\vartheta}_{ii}\left(t\right)x_i\left(t\right)\tanh\rho x_i\left(t\right)+\vartheta_{mii}\dot{\hat{\vartheta}}_{mii}\right),\tag{30}$$

and

$$\dot{V}_{\varphi}\left(\mathbf{x}\left(t\right)\right)=\sum_{n=1}^{\infty}\left(\varrho\varphi_{mii}\left(x_i\left(t\right)\right)x_i\left(t\right)+\varrho\hat{\varphi}_{ii}\left(t\right)x_i\left(t\right)\tanh\rho x_i\left(t\right)+\varphi_{mii}\dot{\hat{\varphi}}_{mii}\right).\tag{31}$$

4.3 Stability analysis of $\dot{V}_{KL}\left(\mathbf{x}\left(t\right)\right)$, $\dot{V}_{\vartheta}\left(\mathbf{x}\left(t\right)\right)$, and $\dot{V}_{\varphi}\left(\mathbf{x}\left(t\right)\right)$

(i) Analysis of $\dot{V}_{KL}\left(\mathbf{x}\left(t\right)\right)$

Since $-\varrho\sum_{n=1}^{\infty}L_{ii}\left(t\right)x_i\left(t\right)\tanh\rho x_i\left(t\right)\le 0$, and let us choose $k_{11}>\frac{1}{2}$, $k_{11}>\frac{\lambda}{\varrho}+\frac{1}{2}$, and $L_{ii}>0$, then $\dot{V}_{KL}\left(\mathbf{x}\left(t\right)\right)\le 0$.

(ii) Analysis of $\dot{V}_{\vartheta}\left(\mathbf{x}\left(t\right)\right)$ and $\dot{V}_{\varphi}\left(\mathbf{x}\left(t\right)\right)$

To show that $\dot{V}_{\vartheta}\left(\mathbf{x}\left(t\right)\right)\le 0$ and $\dot{V}_{\varphi}\left(\mathbf{x}\left(t\right)\right)\le 0$, let us choose $\rho\le 1$, and consider,

$$\begin{aligned}\dot{V}_{\vartheta}\left(\mathbf{x}\left(t\right)\right)&=\sum_{n=1}^{\infty}\left(\varrho\vartheta_{mii}\left(x_i\left(t\right)\right)x_i\left(t\right)+\varrho\hat{\vartheta}_{ii}\left(t\right)x_i\left(t\right)\tanh\rho x_i\left(t\right)+\vartheta_{mii}\dot{\hat{\vartheta}}_{mii}\left(t\right)\right)\\&\le\sum_{n=1}^{\infty}\left(\left|\varrho\vartheta_{mii}\left(x_i\left(t\right)\right)x_i\left(t\right)\right|+\varrho\hat{\vartheta}_{ii}\left(t\right)x_i\left(t\right)\tanh\rho x_i\left(t\right)+\vartheta_{mii}\dot{\hat{\vartheta}}_{mii}\left(t\right)\right)\\&=\sum_{n=1}^{\infty}\left(\left|\varrho\vartheta_{mii}\left(x_i\left(t\right)\right)\right|\left|x_i\left(t\right)\right|+\varrho\hat{\vartheta}_{ii}\left(t\right)x_i\left(t\right)\tanh\rho x_i\left(t\right)+\vartheta_{mii}\dot{\hat{\vartheta}}_{mii}\left(t\right)\right)\\&\le\sum_{n=1}^{\infty}\left(\varrho\vartheta_{mii}\left|x_i\left(t\right)\right|+\varrho\hat{\vartheta}_{ii}\left(t\right)x_i\left(t\right)\tanh\rho x_i\left(t\right)+\vartheta_{mii}\dot{\hat{\vartheta}}_{mii}\left(t\right)\right).\end{aligned}\tag{32}$$

Using the update law $\dot{\hat{\vartheta}}_{mii}(t)$ (24) into (32) gives:

$$\dot{V}_{\vartheta}(\mathbf{x}(t)) \leq \sum_{n=1}^{\infty}\Big(\varrho\vartheta_{mii}|x_i(t)| + \varrho\hat{\vartheta}_{ii}(t)\,x_i(t)\tanh\rho x_i(t) + \vartheta_{mii}(-\varrho|x_i(t))\Big)$$
$$= \sum_{n=1}^{\infty}\varrho\hat{\vartheta}_{ii}(t)\,x_i(t)\tanh\varrho x_i(t) \leq 0, \tag{33}$$

because $\hat{\vartheta}(t) \leq 0$.

In the same way,

$$\dot{V}_{\varphi}(\mathbf{x}(t)) = \textstyle\sum_{n=1}^{\infty}\varrho\hat{\varphi}_{ii}(t)\,x_i(t)\tanh\rho x_i(t) \leq 0. \tag{34}$$

Therefore,

$$\dot{V}(\mathbf{x}(t)) \leq \dot{V}_{KL}(\mathbf{x}(t)) + \dot{V}_{\vartheta}(\mathbf{x}(t)) + \dot{V}_{\varphi}(\mathbf{x}(t)) \leq 0. \tag{35}$$

From (35), it is established that all the state variable trajectories converge to zero and the unknown parameters associated with the uncertainties and external disturbances converge to some constants. It proves that the closed-loop (15) is global asymptotic stable [24]. Thus $\lim_{t\to\infty}||\mathbf{x}(t)|| = 0$.

4.4 Numerical simulations and comparative analysis

This subsection provides numerical simulations to evaluate the robustness and efficiency of the proposed RACC approach (23). The initial states of the MHP chaotic system (2) are taken as $[x_1(0)\quad x_2(0)]^T = [-3.4\quad 2.1]^T$. The actual values of the parameters for which the MHP system is chaotic are set as $\alpha = \frac{4}{3}$, $\beta = 3.776$, $h = \frac{34}{3}$, $\gamma = 4.6 \times 12^{-6}$, and $\omega = 1.8$. The feedback controller gains are chosen as $k_{11} = k_{22} = 2$, and $l_{11} = l_{22} = 1$. The positive real constants $\rho, \lambda, \sigma, \eta, \varrho$, and τ are selected as $\rho = \lambda = 1$, $\sigma = \eta = 0.1, \varrho = 2$, and $\tau = 0.1$. Consequently, in simulations, the following state-dependent and time-dependent disturbances are added to (15), respectively.

$$\begin{array}{c}\vartheta_{11}(x_1(t)) = 0.3sin5x_1(t)\,, \varphi_{11}(t) = 0.2cos(3t)\,,\\ \vartheta_{22}(x_2(t)) = 0.2cos2x_2(t)\,, \varphi_{22}(t) = 0.25sin(4t)\,.\end{array} \tag{36}$$

Example 1: In this example, simulation results (Figs. 3(a-d)) are performed without a control effort. Figs. 3(a-b) illustrate the 2-D phase portraits of the MHP chaotic system with and without time delay, respectively, whereas Figs. 3(c-d) show the behavior of the MHP chaotic systems' state variables with and without time delay, respectively. These figures show that the state variable trajectories keep oscillating in a bounded region. Fig. 4 shows that the state variable trajectories $x_i(t), i = 1, 2$ converge to zero with significantly less active oscillations under the control effort computed using (23). It also demonstrates that the state variable trajectories converge to zero with a short convergence time (0.8 seconds) and good quality of transient performance. Figs. 5(a-c) illustrate the convergence of the adaptation parameters. It is shown that the adaptation parameters $\hat{\alpha}(t)$, $\hat{\beta}(t)$ and $\hat{\gamma}(t)$ with initial values $\hat{\alpha}_0 = 1$, $\hat{\beta}_0 = 0.2$ and $\hat{\gamma}_0 = 0.2$, alternatively converge to their true values, and $\hat{\vartheta}_{ii}(t)$ and $\hat{\varphi}_{ii}(t)$ with initial values $\hat{\vartheta}_{ii0} = 0$ and $\hat{\varphi}_{ii0} = 0$, respectively converge to some constant under the parameters adaptation laws (24).

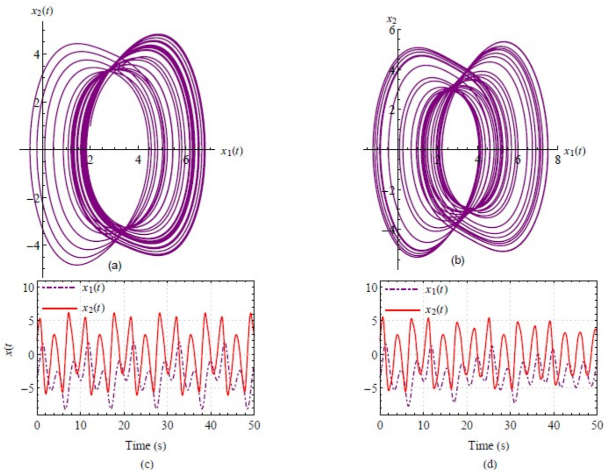

Figure 3. (a) 2-D chaotic attractor of the MHP system with time-delay, (b) 2-D chaotic attractor of the MHP system without time-delay, (c) Transient behavior of the state variable trajectories of the MHP chaotic system with time-delay, and (d) Transient behavior of the state variable trajectories of the MHP chaotic system without time-delay.

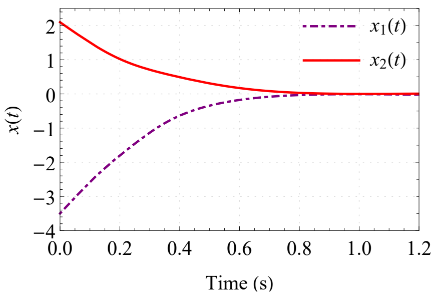

Figure 4. Convergence of the state variable trajectories.

4.5 Comparative study

Example 2: This example re-simulates Example 1 using the controller proposed in the research papers [7, 8]. The control signals $u_1(t)$ and $u_2(t)$ are synthesized by (i) the ASMC technique [7] and adaptive control strategy (ACS) [8], described in (37) and (38), respectively. These control signals in the closed-loop system (15) establish the control of chaos in the uncertain time-delay MHP chaotic system. Assume that the initial conditions, design control parameters, the time-delay τ, feedback gains, unknown state-dependent, and unknown time-dependent disturbances are set the same for the benchmarking study.

(i) The ASMC technique [7]:

$$\mathbf{u}(t) = \begin{cases} u_1(t) = -x_2(t) - k_{11}x_1(t) - l_{11}sig(s_1(t)) \\ u_2(t) = -k_{22}s_2(t) - l_{22}sig(s_2(t)) + \hat{\alpha}(t)x_2(t-\tau) \\ \qquad + \hat{\beta}(t)\,sinx_1(t) - \hat{\gamma}(t)\,cosx_1(t)\,sinx_1(t) - \delta cos\,\omega t, \end{cases} \tag{37}$$

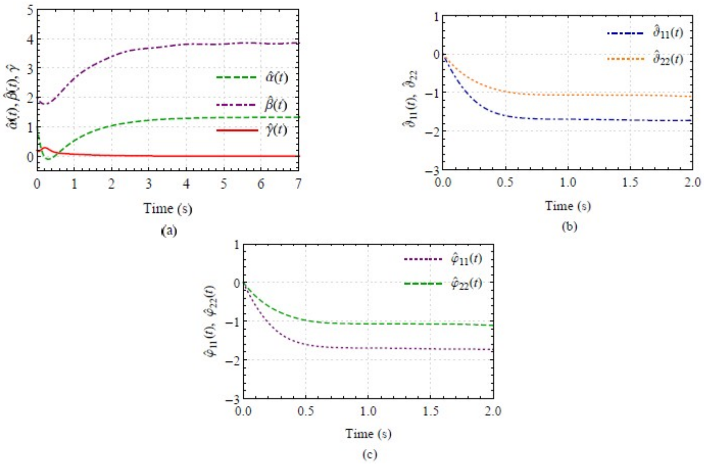

Figure 5. Convergence of the adaptation parameters (a) $\hat{\alpha}(t)$, $\hat{\beta}(t)$, $\hat{\gamma}(t)$, (b) $\hat{\vartheta}_{ii}(t)$, and (c) $\hat{\varphi}_{ii}(t), i = 1, 2$.

where $s_i(t) = \mu_i x_i(t)$ is the switching surface and $\mu_i > 0$ is a real constant.
(ii) The ACS [8]:

$$\mathbf{u}(t) = \begin{cases} u_1(t) = -x_2(t) - k_{11}x_1(t) \\ u_2(t) = -k_{22}x_2(t) + \hat{\alpha}(t)\,x_2(t-\tau) + \hat{\beta}(t)\,sinx_1(t) \\ \qquad - \hat{\gamma}(t)\,cosx_1(t)\,sinx_1(t) - \delta cos\,\omega t \end{cases} \tag{38}$$

As compared to the feedback control approaches [7, 8], some of the advantages of the proposed RACC algorithm (23) are outlined as follows:

(i) In the closed-loop system (15), the control strategies [7, 8] cancel out most of the linear and nonlinear terms, which deteriorate the system dynamics' complexity. Such a linearized feedback closed-loop system performs weak operations, including long time-delay and sudden supply load disturbances [18]. These factors leave adverse effects on the performance of the controlled system, and the system may lose its stability. A hefty control effort is then required to bring back the system to its equilibrium point. In such a situation, the controller may cause the saturation problem. The proposed RACC scheme (23) facilitates the cancellation of a single nonlinear term. Complex controlled industrial systems are safe, efficient, and ensure profitable operations in various practical applications [26].

(ii) Figs. 6(a-b) demonstrate the convergence behavior of the state variable trajectories $x_1(t)$ and $x_2(t)$ by (37) and (38), respectively. From the simulation results given in Fig. 6(a), it is clear that the reported controller (37) achieves the stabilization of the closed-loop system (15) after 1.1 seconds. Figs. 6(b) shows oscillatory behavior, and the state variable trajectories do not achieve a steady state. The amplitude and transient time are two essential features in control systems theory.

(iii) Table 2 compares the convergence rates in this paper and the feedback control approaches [7, 8].

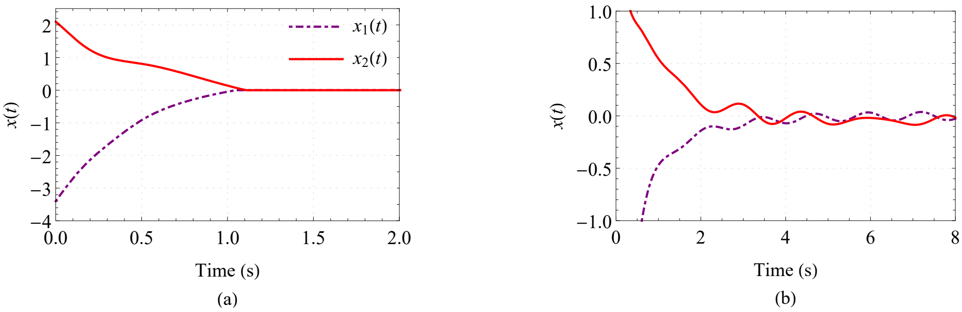

Figure 6. Convergence of the state variable trajectories by (a) ASMC technique (37) and (b) ACS (38).

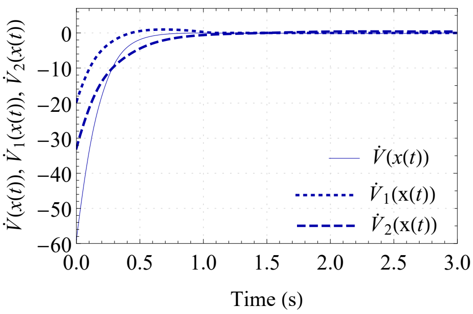

Figure 7. Convergence rates comparison.

From Table 2, the following inequality is obtained:

$$\dot{V}\left(\mathbf{x}\left(t\right)\right) \leq \dot{V}_2\left(\mathbf{x}\left(t\right)\right) \leq \dot{V}_1\left(\mathbf{x}\left(t\right)\right). \tag{39}$$

Fig. 7 compares the rate of convergence of the energy function in the present work and by the control approaches (37-38), it verifies the inequality (39). It shows that the proposed controller (23) accomplishes a rapid dissipation rate of convergence of the energy function to zero than the other two controllers (37-38). Further, it affirms that the proposed RACC approach (23) uses less energy than the other two. Faster convergence rates provide higher accuracy and better disturbance rejection attributes.

(iv) Figs. 8(a-c) illustrate the transient behavior of the control input signals by proposed RACC (23) and feedback control approaches [7, 8], alternatively. These figures show that the feedback control signals (23) are chattering-free. The feedback control strategies [7] exhibit chattering as shown in Fig. 8(b). Though the control signals in (38) are less active than the proposed controller (23), note that the state variable trajectories in Fig. 6(b) do not achieve the steady state and oscillate in the range of $[-0.1,\ 0.1]$. Fig. 4 shows that the state variable trajectories reach the vicinity of zero smoothly in a shorter time than the other two feedback controllers.

Table 2. Comparison of the convergence rates.

Feedback controller	Energy function $V(\mathbf{x}(t))$	Rate of convergence of the energy function $V(\mathbf{x}(t))$
RACC (23)	Eq. (25)	$\dot{V}(\mathbf{x}(t)) \le -\dot{V}_{KL}(\mathbf{x}(t))$
ACS (37)	$V_1(\mathbf{x}(t)) = \frac{1}{2}\mathbf{x}^T(t)\mathbf{x}(t)$ $+\frac{1}{2}\left(\tilde{\alpha}^2(t) + \tilde{\beta}^2(t) + \tilde{\gamma}^2(t)\right)$ $+\frac{\lambda}{2}\int_{t-\tau}^{t} x_2^2(t)\,dt \ge 0$	$\dot{V}_1(\mathbf{x}(t)) \le -\mathbf{x}^T(t)(\mathbf{k}-\lambda)\mathbf{x}(t)$
ASMC (38)	$V_2(\mathbf{x}(t)) = \frac{1}{2}\mathbf{s}^T(t)\mathbf{s}(t)$ $+\frac{1}{2}\left(\tilde{\alpha}^2(t) + \tilde{\beta}^2(t) + \tilde{\gamma}^2(t)\right)$ $+\frac{\lambda}{2}\int_{t-\tau}^{t} s_2^2(t)\,dt \ge 0$	$\dot{V}_2(\mathbf{x}(t)) \le -\mathbf{s}^T(t)(\mathbf{k}-\lambda)\mathbf{s}(t)$ $-\mathbf{L}\lvert\mathbf{s}(t)\rvert$

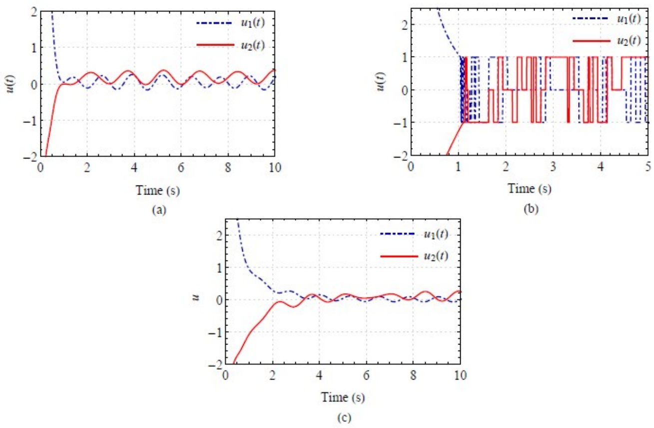

Figure 8. The transient behavior of the control input signals, (a) RACC approach (23), (b) ACS (37), and (c) ASMC technique (38).

§5 Solution to Problem 2

5.1 Controller design

To stabilize the synchronization error system (20) at the origin, Eq. (40) gives the design of the RACC functions.

$$\mathbf{u}(t) = \begin{cases} u_1(t) = -k_{11}e_1(t) - L_{11}(t)\tanh\rho e_1(t) + \left(\hat{\vartheta}_{m11}(t) + \hat{\varphi}_{m11}(t)\right)\tanh\rho e_1(t) \\ u_2(t) = -k_{22}e_2(t) - L_{22}(t)\tanh\rho e_2(t) + \left(\hat{\vartheta}_{m22}(t) + \hat{\varphi}_{m22}(t)\right)\tanh\rho e_2(t), \\ \qquad + \hat{\alpha}(t)e_2(t-\tau) + \hat{\beta}(t)e_1(t) + \dfrac{1}{2}\hat{\gamma}(t) \end{cases} \tag{40}$$

where $L(t) = [L_{ij}(t), L_{ij}(t) = 0 \ for \ i \ne j]_{2\times 2}$ and $L_{ii}(t) = [l_{ii}\left(I_{ii} - \eta e^{-\sigma|e_i(t)|}\right)]_{2\times 2}$, $\hat{\alpha}(t), \hat{\beta}(t), \hat{\gamma}(t),\ \hat{\vartheta}_{mii}(t)$, and $\hat{\varphi}_{mii}(t), i = 1, 2$ are the adaptation parameters. k_{ii} and $L_{ii}(t), i = 1, 2$ are the feedback gains.

5.2 Robust asymptotic stability analysis

Theorem 5.1. If the feedback control signals (40) are applied to the MSS (17-18), and (41) gives the parameter adaptation laws, then the MSS (17-18) realizes the asymptotic stable synchronization.

$$\begin{cases} \dot{\hat{\alpha}}(t) = -\varrho e_2(t-\tau)\, e_2(t)\,, \dot{\hat{\beta}}(t) = -\varrho e_1(t)\, e_2(t)\,, \\ \dot{\hat{\gamma}}(t) = \frac{\varrho}{2}(sin2y_1(t) - sin2x_1(t))\, e_2(t)\,, \\ \dot{\hat{\vartheta}}_{ii}(t) = \dot{\hat{\varphi}}_{ii}(t) = -\varrho|e_i(t)|, \hat{\alpha}(0) = \hat{\alpha}_0, \hat{\beta}(0) = \hat{\beta}_0, \\ \hat{\gamma}(0) = \hat{\gamma}_0, \hat{\vartheta}_{ii}(0) = \hat{\vartheta}_{ii0}, \hat{\varphi}_{ii}(0) = \hat{\varphi}_{ii0}, i = 1, 2, \end{cases} \tag{41}$$

where $\hat{\alpha}_0$, $\hat{\beta}_0$, $\hat{\gamma}_0$, $\hat{\vartheta}_{ii0}$ and $\hat{\varphi}_{ii0}$ are the initial values of $\hat{\alpha}(t)$, $\hat{\beta}(t)$, $\hat{\gamma}(t)$, $\hat{\vartheta}_{ii}(t)$, and $\hat{\varphi}_{ii}(t)$, alternatively.

Proof. Consider the following Lyapunov functional as:

$$V(\mathbf{e}(t)) = \begin{array}{l} \frac{\varrho}{2}\mathbf{e}^T(t)\,\mathbf{e}(t) + \frac{1}{2}\left(\hat{\alpha}^2(t) + \hat{\beta}^2(t) + \hat{\gamma}^2(t)\right) + \frac{1}{2}\sum_{n=1}^{\infty}\left(\tilde{\vartheta}_{mii}(t)\,\vartheta_{mii} + \tilde{\varphi}_{mii}(t)\,\varphi_{mii}\right) \\ + \frac{\lambda}{2}\int_{t-\tau}^{t} e_2^2(t)\, dt \geq 0, \end{array} \tag{42}$$

provided $|\tilde{\vartheta}_{mii}(t)| \leq \vartheta_{mii}$ and $|\tilde{\varphi}_{mii}(t)| \leq \varphi_{mii}$, where $\tilde{\vartheta}_{mii}(t) = \vartheta_{mii} + \hat{\vartheta}_{mii}(t)$, $\tilde{\varphi}_{mii}(t) = \varphi_{mii} + \hat{\varphi}_{mii}(t)$, and $\tilde{\alpha}(t) = \hat{\alpha}(t) - \alpha$, $\tilde{\beta}(t) = \hat{\beta}(t) - \beta$, and $\tilde{\gamma}(t) = \hat{\gamma}(t) - \gamma$. The derivative of (43) along (20) and substituting the control inputs (40) yields:

$$\begin{aligned} &\dot{V}(\mathbf{x}(t)) = \varrho(e_1(t)\, e_2(t)) - \varrho\sum_{n=1}^{\infty} k_{ii} e_i^2(t) - \varrho\sum_{n=1}^{\infty} L_{ii}(t)\, e_i(t) \tanh\rho e_i(t) \\ &+ \varrho\hat{\alpha}(t)\, e_2(t-\tau)\, e_2(t) - \varrho\alpha e_2(t-\tau)\, e_2(t) - \varrho\beta e_1(t)\, e_2(t)\, cos\theta \\ &+ \varrho\hat{\beta} e_1(t)\, e_2(t) + \frac{1}{2}\varrho\gamma(sin2y_1(t) - sin2x_1(t))\, e_2(t) \\ &- \frac{1}{2}\varrho\hat{\gamma}(t)(sin2y_1(t) - sin2x_1(t))\, e_2(t) + \varrho\sum_{n=1}^{\infty}(\vartheta_{ii}(e_i(t)) + \varphi_{ii}(t))\, e_i(t) \\ &+ \sum_{n=1}^{\infty}\left(\vartheta_{mii}\dot{\hat{\vartheta}}_{ii}(t) + \varphi_{ii}\dot{\hat{\varphi}}_{mii}(t)\right) + \varrho\sum_{n=1}^{\infty}\left(\hat{\vartheta}_{mii}(t) + \hat{\varphi}_{mii}(t)\right) e_i(t) \tanh\rho e_i(t) \\ &+ \lambda e_2^2(t) + \varrho e_2(t-\tau)\, e_2^2(t) + \tilde{\alpha}(t)\,\dot{\hat{\alpha}}(t) + \tilde{\beta}(t)\,\dot{\hat{\beta}}(t) + \tilde{\gamma}(t)\,\dot{\hat{\gamma}}(t)\,. \end{aligned} \tag{43}$$

Remark 5.1. The rest of the procedure for the robust stability analysis is similar to that given in subsections 4.2 and 4.3. Therefore, the details are omitted here.

5.3 Numerical simulations

This subsection provides numerical simulations to evaluate the robustness and efficiency of the proposed RACC approach (40) in synchronizing two identical MHP chaotic systems (17-18) with time delay. The initial states of the MSS (17-18) are taken as $[x_1(0) \quad x_2(0)]^T = [-3.4 \quad 2.1]^T$ and $[y_1(0) \quad y_2(0)]^T = [0.78 \quad -2.9]^T$. The feedback controller gains are chosen as $k_{11} = k_{22} = 10$, and $l_{11} = l_{22} = 1$, and the positive real constants $\rho, \lambda, \sigma, \eta, \varrho$, and τ are selected as $\rho = \lambda = 1$, $\sigma = \eta = 0.1$, $\varrho = 2$, and $\tau = 0.1$. Consequently, in simulations, the following state-dependent and time-dependent disturbance signals (44) are added to the MSS (17-18), respectively.

$$\begin{aligned}
&\hat{\vartheta}_{11}^{M}(x_1(t)) = -0.3sin3x_1(t), \hat{\vartheta}_{22}^{M}(x_2(t)) = -0.2cos2x_2(t),\\
&\hat{\vartheta}_{11}^{S}(y_1(t)) = 0.25cos2y_1(t), \hat{\vartheta}_{22}^{S}(y_2(t)) = -0.35cos6y_2(t), \varphi_{11}^{M}(t) = -0.2cos5t,\\
&\varphi_{22}^{M}(t) = 0.25sin4t, \varphi_{11}^{S}(t) = -0.2cos3t, \varphi_{22}^{S}(t) = 0.25sin3t.
\end{aligned} \tag{44}$$

Example 3: In this example, Fig. 9(a) shows the transient behavior of the synchronization error vector trajectories $e_i(t), i = 1, 2$ without considering the feedback controller in (40). Fig. 9(b) demonstrates the convergence behavior of the synchronization error vector trajectories $e_i(t), i = 1, 2$ using the RACC effort computed in (40). Fig. 9(b) illustrates that the error trajectories converge to zero with a short convergence time (0.3 seconds) and good quality of transient performance.

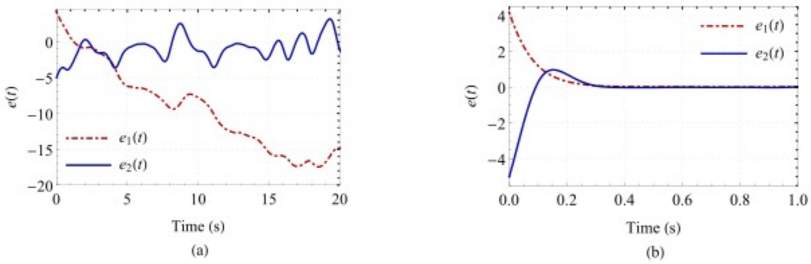

Figure 9. (a) Transient behavior of the error trajectories without control input, and (b) convergence behavior of the synchronization error trajectories.

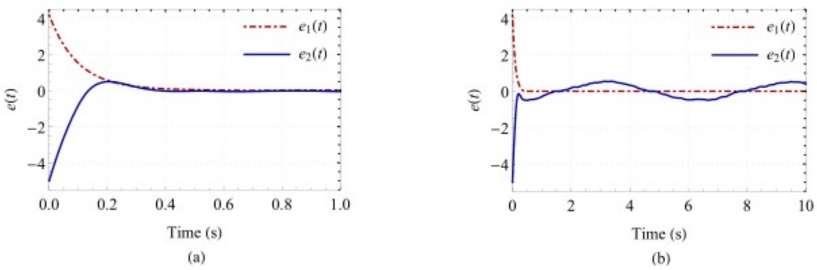

Figure 10. The convergence of the error signals $e_i(t), i = 1, 2$ by (a) ACS (45) and (b) ASMC technique (46).

5.4 Comparatve study

Example 4: This example re-simulates Example 3 using the feedback controllers proposed in [8, 9] to analyze the comparative performance and efficiency of the proposed controller (40). The control signals $u_1(t)$ and $u_2(t)$ synthesized by the ACS [8], and the ASMC technique [9] are described in (46) and (47), respectively. These feedback controllers are applied to the

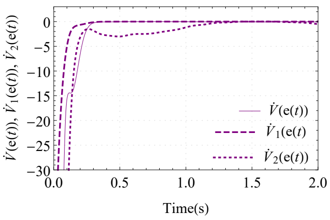

Figure 11. Convergence rates comparison.

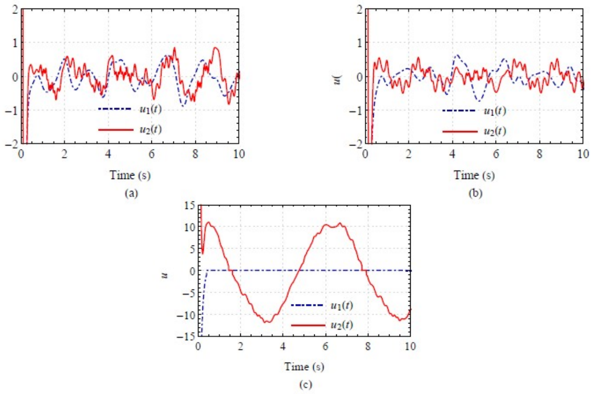

Figure 12. The transient behavior of the feedback control inputs, (a) RACC approach (40), (b) ACS (45), and (c) ASMC technique (46).

closed-loop system (22) to establish synchronization (17-18). For the benchmark, assume that initial conditions and controller design parameters are the same for both systems.

(i) The ACS [8]:

$$\mathbf{u}(t) = \begin{cases} u_1(t) = -e_2(t) - k_{11}e_1(t) \\ u_2(t) = -k_{22}e_2(t) + \hat{\alpha}(t)\,e_2(t-\tau) + \hat{\beta}(t)\,(siny_1(t) - sinx_1(t)) \\ \qquad - \hat{\gamma}(t)\,(cosy_1(t)\,siny_1(t) - cosx_1(t)\,sinx_1(t)), \end{cases} \tag{45}$$

(ii) The ASMC technique [9]:

$$\mathbf{u}(t) = \begin{cases} u_1(t) = -e_2(t) - k_{11}e_1(t) - l_{11}sgn(s_1(t)) \\ u_2(t) = -k_{22}e_2(t) - l_{22}sgn(s_2(t)) + \hat{\alpha}(t)\,e_2(t-\tau) \\ \qquad + \hat{\beta}(t)\,(siny_1(t) - sinx_1(t)) \\ \qquad - \hat{\gamma}(t)\,(cosy_1(t)\,siny_1(t) - cosx_1(t)\,sinx_1(t)) \end{cases} \tag{46}$$

where $s_i(t) = \mu_i e_i(t), i = 1, 2$ is the sliding surface and $\mu_i > 0$ is any real constant.

Figs. 10(a-b) depict error vector trajectories convergence behavior accomplished by the adaptive controller in (45) and the ASMC technique in (46), respectively. These figures demonstrate that the ACS (45) establishes the synchronization in 0.7 seconds with reduced oscillations. Fig. 10(b) shows oscillatory behavior, and the error vectors do not achieve a steady state and oscillate in the range of $[-0.5,\ 0.5]$. Table 3 compares the convergence rates in this paper and by the synchronization control approaches [8, 9].

Table 3. Comparison of the convergence rates.

Feedback controller	Energy function $V(\mathbf{x}(t))$	Rate of convergence of the energy function $V(\mathbf{x}(t))$
RACC (40)	Eq. (42)	$\dot{V}(\mathbf{e}(t)) \leq -\dot{V}_{KL}(\mathbf{e}(t))$
ACS (45)	$V_1(\mathbf{e}(t)) = \frac{1}{2}\mathbf{e}^T(t)\mathbf{e}(t)$ $+\frac{1}{2}\left(\tilde{\alpha}^2(t) + \tilde{\beta}^2(t) + \tilde{\gamma}^2(t)\right)$ $+\frac{\lambda}{2}\int_{t-\tau}^{t} e_2^2(t)\,dt \geq 0$	$\dot{V}_1(\mathbf{e}(t)) \leq -\mathbf{e}^T(t)(\mathbf{k}-\lambda)\mathbf{e}(t)$
ASMC (46)	$V_2(\mathbf{e}(t)) = \frac{1}{2}\mathbf{s}^T(t)\mathbf{s}(t)$ $+\frac{1}{2}\left(\tilde{\alpha}^2(t) + \tilde{\beta}^2(t) + \tilde{\gamma}^2(t)\right)$ $+\frac{\lambda}{2}\int_{t-\tau}^{t} s_2^2(t)\,dt \geq 0$	$\dot{V}_2(\mathbf{e}(t)) \leq -\mathbf{s}^T(t)(\mathbf{k}-\lambda)\mathbf{s}(t)$ $-\mathbf{L}\lvert\mathbf{s}(t)\rvert$

The inequality (47) is obtained using Table 3.

$$\dot{V}(\mathbf{e}(t)) \leq \dot{V}_2(\mathbf{e}(t)) \leq \dot{V}_1(\mathbf{e}(t)). \tag{47}$$

The simulation results in Fig. 11 verify the inequality (47), where $\dot{V}(\mathbf{e}(t))$ determines the rate of convergence. Fig. 11 and inequality (47) confirm that the synchronization rate of convergence in the present work is faster than the others [8, 9]. Figs. 12(a-c) illustrate the transient behavior of the feedback terms in the proposed RACC approach (40) and by (45-46). These figures show that the control input signals in the proposed RACC strategy (40) are less active than (46). Though the ACS (45) has reduced oscillations compared to the proposed RACC approach (40), the synchronization error vectors remain oscillatory and do not achieve the steady state.

§6 Conclusions

This paper proposes a robust adaptive continuous-time control strategy that investigates the control and synchronization of chaos in the uncertain horizontal platform chaotic system with time delay. The proposed controllers establish oscillation-free convergence of the state variable and synchronization error trajectories to the origin with a shorter transient time and faster convergence rates. The Lyapunov stability theory proves the robust asymptotic stability of the closed-loop at the origin. The paper gives a detailed analysis of the proposed control strategy. This paper also provides parameter adaptation laws that confirm the uncertain parameters' convergence to some constant values. Numerical simulations further validate the theoretical findings. The modified version of the proposed controller will be analyzed for the finite-time suppression and synchronization of fractional-order horizontal platform chaotic systems with uncertain parameters and time delay.

Declarations

Conflict of interest The authors declare no conflict of interest.

References

[1] Y C Hung, C K Hu. *Chaotic communication via temporal transfer entropy*, Phys Rev Lett, 2018, https://doi.org/10.1103/PhysRevLett.101.244102.

[2] Z Zhao, X Song. *Bifurcation and complexity in a ratio-dependent predator-prey chemostat with pulsed input*, Appl Math J Chinese Univ Ser B, 2007, 22(4): 379-387.

[3] R Luo, H Su. *Finite-time control and synchronization of a class of systems via the twisting controller*, Chinese J Phys, 2017, 55(6): 2199-2207.

[4] D Hu, L Hu, Y Yan. *Optimization methodology for control strategy of parallel hybrid electric vehicle based on chaos prediction*, AIP Advances, 2018, 8(11), https://doi.org/10.1063/1.5055644.

[5] C Wu, K Song, H Xie. *Control of the common rail pressure in gasoline engine through an extended state observer based MPC*, Cont Theo Tech, 2019, 17(2): 156-166.

[6] W Liu, D Cai. *Bifurcation, chaos analysis and control in a discrete-time predator-prey system*, Adv Diff Equa, 2019, 11, https://doi.org/10.1186/s13662-019-1950-6.

[7] R Farid, A Ibrahom, B Zalam. *Adaptive Sliding Mode Control for a Class of Chaotic Systems*, AIP Conference Proceedings, 2015, 1653(1), https://doi.org/10.1063/1.4914229.

[8] S S Sajjad, D Baleanu, A Jajarmi, H M Pirouz. *A new adaptive synchronization and hyperchaos control of a biological snap oscillator*, Chaos Solit Fract, 2020, 138, https://doi.org/10.1016/j.chaos.2020.109919.

[9] A Khan, S Kumar. *Measuring chaos and synchronization of chaotic satellite systems using sliding mode control*, Optim Cont App Meth, 2018, 39(5): 1-13.

[10] I Ahmad, M Shafiq, M Alsawalha. *Globally exponential multi switching-combination synchronization control of chaotic systems for secure communications*, Chinese J Phys, 2018, 56(3): 974-987.

[11] P P Singh, B K Roy. *Microscopic chaos control of chemical reactor system using nonlinear active plus proportional integral sliding mode control technique*, The European Phy J: Special Topics, 2019, 228: 168-184.

[12] T Yu, H Wang, D Cao. *Synchronization of delayed neural networks with hybrid coupling via impulsive control*, Trans Instit Measur Cont, 2019, 41(13): 1-11.

[13] A Saaban, A Ibrahim, M Shahzad, I Ahmad. *Identical synchronization of a new chaotic system via nonlinear control and linear active control techniques: A Comparative Analysis*, Int J Hyb Inform Technology, 2014, 7(1): 211-224.

[14] N S Pai, H T Yau. *Suppression of chaotic behavior in horizontal platform systems based on an adaptive sliding mode control scheme*, Commun Non Sci Numer Simul, 2011, 16(1): 133-143.

[15] M P Aghababa, H P Aghababa. *Synchronization of mechanical horizontal platform systems in finite-time*, App Math Model, 2012, 36: 4579-4591.

[16] M L Hung, H T Yau. *Circuit implementation and synchronization control of chaotic horizontal platform systems by wireless sensors*, Math Prob Engin, 2013, 2013(5), https://doi.org/10.1155/2013/903584.

[17] M P Aghababa. *Chaotic behavior in fractional-order horizontal platform systems and its suppression using a fractional finite-time control strategy*, J Mech Sci Tech, 2014, 28(5): 1875-1880.

[18] W Xiang, Y Sun, C Yang. *Fuzzy adaptive prescribed performance control of uncertain horizontal platform system with uncertain control gain*, Math Prob Engin, 2015, https://doi.org/10.1155/2015/896382.

[19] I Ahmad, M Shafiq. *Oscillation free robust adaptive synchronization of chaotic systems with parametric uncertainties*, Trans Instit Measur Cont, 2020, 42(11): 1977-1996.

[20] I Ahmad, A Saaban, A Ibrahim, M Shahzad. *Reduced-order synchronization of time-delay chaotic systems with known and unknown parameters*, OPTIK, 2016, 127(13): 5506-5514.

[21] K Rajagopal, P Duraisamy, R Weldegiorgis, A Karthikeyan. *Multistability in horizontal platform system with and without time delays*, Shock and Vibration, 2018, https://doi.org/10.1155/2018/1092812s.

[22] M Shahzad, I Ahmad, A Saaban, A Ibrahim. *Adaptive control to synchronize and anti-synchronize two identical time-delay Bhalekar-Gejji chaotic systems with unknown parameters*, Int J Autom Control, 2015, 9(3): 211-227.

[23] W Duan, Y Li, J Chen, L Jiang. *New results on stability analysis of uncertain neutral-type Lur'e systems derived from a modified Lyapunov-Krasovskii functional*, Complexity, 2019, https://doi.org/10.1155/2019/1706264.

[24] H K Khalil. *Nonlinear Systems*, Prentice-Hall, New Jersey, 2002.

[25] J K Merikoskia, M Halmetoja, T Tossavainen. *Means and the mean value theorem*, Int J Math Educ Sci Tech, 2009, 40(6): 729-740.

[26] Z Gao, S K Nguang, D X Kong. *Advances in modeling, monitoring, and control for complex industrial systems*, Complexity, 2019, 2019, https://doi.org/10.1155/2019/2975083.

[1]Department of Preparatory Studies Centre, University of Technology and Applied Sciences, Nizwa, Oman.

[2]Department of Electrical and Computer Engineering, Sultan Qaboos University, Oman.

Email: iak_2000plus@yahoo.com